

A novel technique for determining luminosity in electron-scattering/positron-scattering experiments from multi-interaction events

A. Schmidt^{a,*}, C. O'Connor^a, J. C. Bernauer^a, R. Milner^a

^aMassachusetts Institute of Technology, Laboratory for Nuclear Science, Cambridge, MA, USA

Abstract

The OLYMPUS experiment measured the cross-section ratio of positron-proton elastic scattering relative to electron-proton elastic scattering to look for evidence of hard two-photon exchange. To make this measurement, the experiment alternated between electron beam and positron beam running modes, with the relative integrated luminosities of the two running modes providing the crucial normalization. For this reason, OLYMPUS had several redundant luminosity monitoring systems, including a pair of electromagnetic calorimeters positioned downstream from the target to detect symmetric Møller and Bhabha scattering from atomic electrons in the hydrogen gas target. Though this system was designed to monitor the rate of events with single Møller/Bhabha interactions, we found that a more accurate determination of relative luminosity could be made by additionally considering the rate of events with both a Møller/Bhabha interaction and a concurrent elastic ep interaction. This method was improved by small corrections for the variance of the current within bunches in the storage ring and for the probability of three interactions occurring within a bunch. After accounting for systematic effects, we estimate that the method is accurate in determining the relative luminosity to within 0.36%. This precise technique can be employed in future electron-proton and positron-proton scattering experiments to monitor relative luminosity between different running modes.

Keywords: OLYMPUS, electron scattering, storage ring, luminosity, Møller, Bhabha, calorimeter

1. Introduction

The OLYMPUS experiment [1] measured the ratio of positron-proton to electron-proton elastic scattering cross-sections for a 2.01 GeV beam energy over a range of scattering angles [2]. The analysis depended on the accurate (better than 1%) determination of the relative integrated luminosity between positron-beam running mode and electron-beam running mode. Three luminosity monitoring systems were implemented for the experiment, of which one was a pair of Symmetric Møller/Bhabha (SYMB) calorimeters, designed to use the rate of symmetric scattering from the atomic electrons in the hydrogen target to extract luminosity [3]. Since the Møller and Bhabha scattering cross-sections can be calculated precisely using quantum electrodynamics, this method was expected to have high performance. Møller and Bhabha calorimeters had previously been used successfully for luminosity monitoring with the HERMES experiment [4].

Unfortunately, this method turned out to be ill-suited for the needs of OLYMPUS. Whereas HERMES typically needed the relative luminosity between running modes with two different beam or target polarization states using the same beam species, OLYMPUS required the relative luminosity between running modes with different beam species. Since the Møller and Bhabha differential cross-sections have different angular dependences close to the symmetric angle, this method required

control of the calorimeter acceptance to a better degree than was possible, even with sophisticated simulations. We estimated the accuracy of the relative luminosity determination from SYMB to be on the order of 4%.

Nevertheless, we developed an alternate method to determine the relative luminosity from the SYMB data, achieving an accuracy of 0.36% by comparing the rate of symmetric Møller/Bhabha events to the rate of a specific type of multi-interaction event (MIE). In this specific type of MIE, a symmetric Møller/Bhabha interaction occurs simultaneous to an elastic lepton-proton scattering event in which the lepton enters one of the two calorimeters. While the rate of Møller/Bhabha events scales with luminosity, the MIE rate scales with luminosity squared, and by taking a ratio, the luminosity can be recovered. This MIE method has three principal advantages that make it robust against many systematic effects:

1. The important quantity is a ratio of rates rather than a single rate, canceling some systematics,
2. The ratio is nearly the same in both electron and positron modes,
3. There is a reduced burden on acceptance simulations.

In this paper, we present a derivation of the MIE method, estimate its associated systematic accuracy for OLYMPUS, and discuss how it might be useful for luminosity monitoring in future experiments.

*Corresponding author

Email address: schmidta@mit.edu (A. Schmidt)

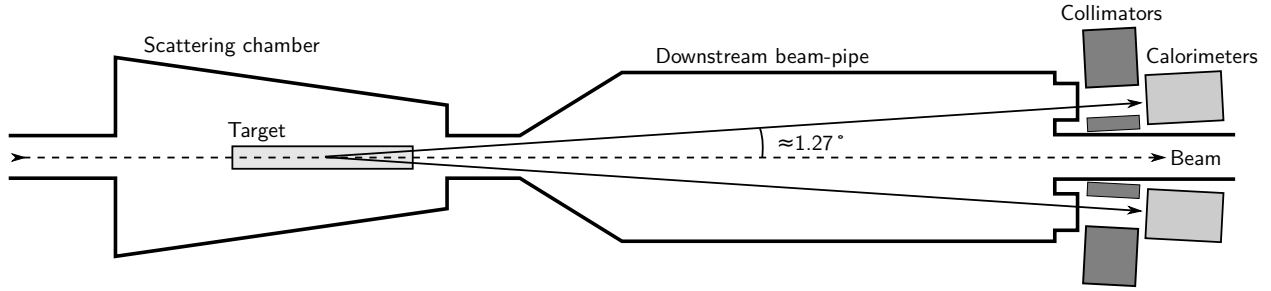


Figure 1: The SYMB calorimeters were positioned approximately 3 m downstream from the target, on either side of the beamline, as seen in this schematic (not to scale).

2. The OLYMPUS Experiment

The OLYMPUS experiment collected data at the DORIS storage ring, at DESY, Hamburg, in 2012. DORIS was capable of storing both electron and positron beams, and, in OLYMPUS, the beam species was switched approximately once per day. Determining the relative integrated luminosity of the data from the two different beam species was crucial for the OLYMPUS measurement.

OLYMPUS operated with a fixed hydrogen gas target. The SYMBs were positioned approximately 3 m downstream from the target, at an approximate scattering angle of 1.27° . This corresponded to the symmetric angle for Møller and Bhabha scattering at the beam energy of 2.01 GeV. The two calorimeters were placed on either side of the beam line in order to detect both final state leptons in coincidence. Fig. 1 shows a schematic of calorimeter placement relative to the target and beamline. Relevant distances and angles, determined from the OLYMPUS optical survey, are given in Table 1.

Table 1: Relevant geometric parameters for the SYMB calorimeters

Parameter	Value
Dist. to upstream face of collimator	2992 mm
Dist. to upstream face of calorimeter	3117 mm
Collimator thickness	100 mm
Radius of collimator aperture	10.25 mm
Angle to center of left collimator aperture	1.32°
Angle to center of right collimator aperture	1.28°
Orientation of left collimator aperture	1.30°
Orientation of right collimator aperture	1.22°
Møller-Bhabha symmetric angle	1.27°

There were two other luminosity monitoring systems in OLYMPUS in addition to the SYMBs. The first was a pair of forward tracking telescopes, which monitored the rate of forward lepton-proton scattering. This method of determining luminosity was relative to the asymmetry, if any, between the electron-proton and positron-proton cross-sections—such as that caused by hard two-photon exchange (TPE)—at the forward scattering angle. However, given a luminosity determination from the SYMBs, the forward tracking telescopes could make a determination of hard TPE. This determination was reported in the OLYMPUS results [2]. The second system was

the OLYMPUS slow control system, which recorded the beam current in the storage ring, the flow rate of hydrogen to the target, and the target temperature, which could be combined into a luminosity determination. This method was only accurate to the order of 3%, but had the advantage that it could be made online during data taking, without any simulation or track reconstruction.

The SYMB data were digitized using fast histogramming cards, whose acquisition time was less than the ≈ 100 ns bunch separation time at DORIS. The system was dead-time free. The cards provided two-dimensional histograms, in which one axis corresponded to the energy deposited in the left calorimeter and the other axis corresponded to the energy of the right calorimeter. Each fill of the histogram corresponded to one beam bunch passing through the target. The SYMB data consisted of three histograms, one triggered on the left calorimeter, one triggered on the right calorimeter, and one triggered on left-right coincidences. The three histograms had different dynamic ranges. The dynamic range of the coincidence histogram was optimized to cover the energy range of symmetric Møller/Bhabha events. The left- and right-triggered histograms, which were intended as diagnostics, had larger dynamic ranges to cover forward-going elastic ep events. By chance, the dynamic range of the left-triggered histogram was large enough to include events of more than 3 GeV, permitting the analysis discussed in this work. The left-triggered histogram for a subset of data is shown in Fig. 2. There are several dense areas—signal peaks—that correspond to specific processes. The most prominent is due to symmetric Møller and Bhabha scattering, which deposits approximately 1 GeV in both the left and the right calorimeters.

3. Derivation

In this derivation, we consider three types of events of interest. In symmetric Møller/Bhabha events, denoted ee , 1 GeV of energy is deposited in each calorimeter. We denote elastic lepton-proton interactions in which the lepton deposits 2 GeV in the left calorimeter with $ep \rightarrow L$. We denote elastic lepton-proton interactions in which the lepton deposits 2 GeV in the right calorimeter with $ep \rightarrow R$. Since the energy depositions in GeV are approximately integer values, we will use a coordinate system (L, R) to label signal peaks. For example, peak $(1, 3)$ refers to the signal peak with 1 GeV deposited in the left and 3 GeV deposited in the right.

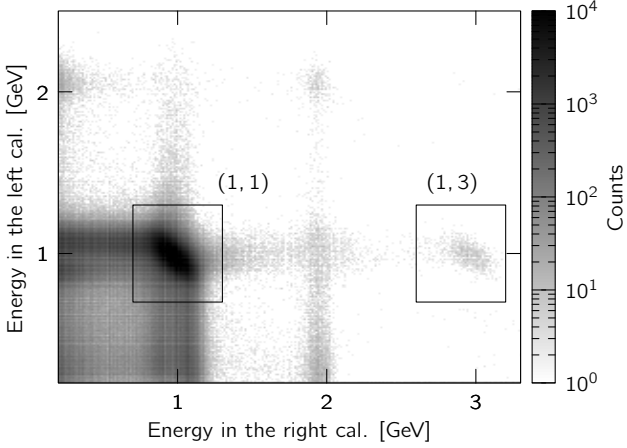


Figure 2: Luminosity can be extracted from the ratio of (1, 3) MIE events (in the right box) to single (1, 1) Møller/Bhabha events (in the left box).

Since the number of beam particles in a bunch is large (order 10^{10}) while the probability of an interaction occurring in a given bunch is small, the probability of having N interaction in a bunch with integrated luminosity \mathcal{L}_j follows a Poisson distribution,

$$P(N) = \frac{e^{-\sigma\mathcal{L}_j}(\sigma\mathcal{L}_j)^N}{N!}, \quad (1)$$

where σ is the cross-section for an interaction. The probability for a bunch crossing to result in an event of form (1, 1) is:

$$P(1, 1) = P_{ee}(1) \times P_{ep \rightarrow L}(0) \times P_{ep \rightarrow R}(0) \quad (2)$$

$$= e^{-\mathcal{L}_j(\sigma_{ee} + \sigma_{ep \rightarrow L} + \sigma_{ep \rightarrow R})} \times \sigma_{ee}\mathcal{L}_j \quad (3)$$

$$= e^{-\mathcal{L}_j\sigma_{\text{tot}}} \times \sigma_{ee}\mathcal{L}_j, \quad (4)$$

where we define $\sigma_{\text{tot}} \equiv \sigma_{ee} + \sigma_{ep \rightarrow L} + \sigma_{ep \rightarrow R}$. In the same way, we can write the probability for energy deposition of the form (1, 3):

$$P(1, 3) = P_{ee}(1) \times P_{ep \rightarrow L}(0) \times P_{ep \rightarrow R}(1) \quad (5)$$

$$= e^{-\mathcal{L}_j(\sigma_{ee} + \sigma_{ep \rightarrow L} + \sigma_{ep \rightarrow R})} \times \sigma_{ee}\sigma_{ep \rightarrow R}\mathcal{L}_j^2 \quad (6)$$

$$= e^{-\mathcal{L}_j\sigma_{\text{tot}}} \times \sigma_{ee}\sigma_{ep \rightarrow R}\mathcal{L}_j^2. \quad (7)$$

Over a run period with N_b bunches crossing the target, the expected number of events, N , in a given signal peak can be found by summing the probabilities over each bunch (assuming N_b is sufficiently large):

$$N_{(1,1)} = \sum_{j=0}^{N_b} P(1, 1) = \sum_{j=0}^{N_b} \left[e^{-\mathcal{L}_j\sigma_{\text{tot}}} \times \sigma_{ee}\mathcal{L}_j \right], \quad (8)$$

$$N_{(1,3)} = \sum_{j=0}^{N_b} P(1, 3) = \sum_{j=0}^{N_b} \left[e^{-\mathcal{L}_j\sigma_{\text{tot}}} \times \sigma_{ee}\sigma_{ep \rightarrow R}\mathcal{L}_j^2 \right]. \quad (9)$$

Since $\mathcal{L}_j\sigma_{\text{tot}} \ll 1$, we can recast the exponentials as a power series, which we can truncate. Dividing the two rates, dropping terms beyond first order in $\mathcal{L}_j\sigma_{\text{tot}}$, and using $\mathcal{L} = \sum_j^{N_b} \mathcal{L}_j$ to

represent the integrated luminosity of the entire run period, we get:

$$\frac{N_{(1,3)}}{N_{(1,1)}} = \frac{\sigma_{ep \rightarrow R} \sum_{j=0}^{N_b} \mathcal{L}_j^2 [1 - \mathcal{L}_j\sigma_{\text{tot}}]}{\sum_{j=0}^{N_b} \mathcal{L}_j [1 - \mathcal{L}_j\sigma_{\text{tot}}]}, \quad (10)$$

$$= \frac{\sigma_{ep \rightarrow R} N_b [\langle \mathcal{L}_j^2 \rangle - \sigma_{\text{tot}} \langle \mathcal{L}_j^3 \rangle]}{[\mathcal{L} - N_b \sigma_{\text{tot}} \langle \mathcal{L}_j^2 \rangle]}, \quad (11)$$

$$= \frac{\sigma_{ep \rightarrow R} N_b}{\mathcal{L}} [\langle \mathcal{L}_j^2 \rangle - \sigma_{\text{tot}} \langle \mathcal{L}_j^3 \rangle] \left[1 + \frac{N_b}{\mathcal{L}} \sigma_{\text{tot}} \langle \mathcal{L}_j^2 \rangle \right], \quad (12)$$

The variance in luminosity per bunch, v_b , is equal to $\langle \mathcal{L}_j^2 \rangle - \langle \mathcal{L}_j \rangle^2$, or equivalently $\langle \mathcal{L}_j^2 \rangle - \mathcal{L}^2/N_b^2$. Using this substitution, dropping the σ_{tot}^2 term, and rearranging we arrive at:

$$\mathcal{L} = \frac{N_{(1,3)}N_b}{N_{(1,1)}\sigma_{ep \rightarrow R}} - \frac{v_b N_b^2}{\mathcal{L}} - N_b \sigma_{\text{tot}} \left\{ \left(\frac{v_b N_b}{\mathcal{L}} + \frac{\mathcal{L}}{N_b} \right)^2 - \frac{\langle \mathcal{L}_j^3 \rangle N_b}{\mathcal{L}} \right\}. \quad (13)$$

Eq. 13 shows that luminosity can be estimated from a main term, $N_{(1,3)}N_b/N_{(1,1)}\sigma_{ep \rightarrow R}$, with some corrections. In this derivation, only terms to first order in $\mathcal{L}\sigma_{\text{tot}}$, have been kept, but, if necessary, corrections can be calculated to arbitrary order.

Let us consider the meaning of the correction terms. The first correction term, $v_b N_b^2/\mathcal{L}$, describes the effect of luminosity variance between bunches. High-luminosity bunches are more likely to have multi-interaction events than low-luminosity bunches. If there is variance between the bunches, this will have an effect on the luminosity determination. The second correction term, which has a leading factor of σ_{tot} , accounts for the fact that there may be three interactions in a bunch crossing. Some small fraction of would-be (1,3) events will fall outside of the (1,3) peak because of additional energy deposited by a third interaction in the same bunch.

Fig. 3 shows the scale for these correction terms relative to the total luminosity, for a typical week of running. The variance term is highly species-dependent, and corrects the extracted luminosity by a few percent. This term is absolutely necessary to achieve percent-level accuracy desired for OLYMPUS. The correction for three-interactions per bunch is smaller, on the order of one to two tenths of a percent. Subsequent higher-order terms are even smaller and can be safely neglected.

Eq. 13 is not the result of solving for \mathcal{L} ; luminosity appears in both sides of the equation. However, \mathcal{L} , v_b , and $\langle \mathcal{L}_j^3 \rangle$ appear only in the correction terms. Since these terms are already small, there is little residual error in using a rough estimate of the luminosity to calculate these terms. For the purposes of OLYMPUS, the slow control system was suitable for estimating \mathcal{L} , v_b , and $\langle \mathcal{L}_j^3 \rangle$, as well as N_b that appear in the right side of the equation. The cross-sections $\sigma_{ep \rightarrow L}$, $\sigma_{ep \rightarrow R}$, and σ_{ee} were estimated using simulations. The yields $N_{(1,1)}$ and $N_{(1,3)}$ were, naturally, taken from the calorimeter data.

The luminosity determination in this work relies on the (1, 3) signal peak, visible only in the left-triggered histogram, but it

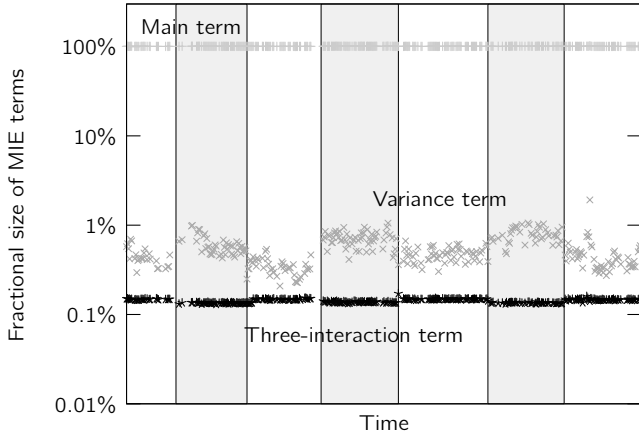


Figure 3: The variance term modified the luminosity by slightly less than a percent, while the three-interaction term was closer to a 0.1% correction. The background shading shows the different beam species; a white background indicates electron beam running, while a light gray background indicates positron beam running.

Table 2: Contributions to the systematic uncertainty

Uncertainty	Value (%)
Statistics	0.10
Beam Position Monitors	0.21
Magnetic Field at Target	0.20
Collimator Geometry	0.13
Event Selection	0.10
Downstream Magnetic Field	0.05
Higher Order Corrections	0.05
Radiative Corrections	0.03
Total	0.36
Beam Energy	0.10
Total incl. Beam Energy	0.37

would be equally possible to extract luminosity from counts in the (3, 1) peak. This was not possible for OLYMPUS because the (3, 1) signal peak was outside of the dynamic ranges of all three SYMB data histograms. If a luminosity monitor were designed around this principle, a comparison of the (1, 3) and (3, 1) rates would provide a valuable cross check.

4. Systematics

In this section, we present our estimate for the systematic uncertainty of the MIE method as applied in OLYMPUS. The principal source of uncertainty was the use of a simulation to estimate $\sigma_{ep \rightarrow R}$. Any inaccuracy in the simulation contributed to error in the relative luminosity determination. This uncertainty estimation is specific to the OLYMPUS simulation as implemented in the OLYMPUS analysis. If the MIE method were used in a future experiment, it may prove more or less accurate depending on that experiment's simulation.

The sources of systematic uncertainty in the simulation can be divided into several classes, which we will address in turn.

Our estimates of the uncertainty contributed by each of these classes is shown in Table 2.

4.1. Beam Position Monitors

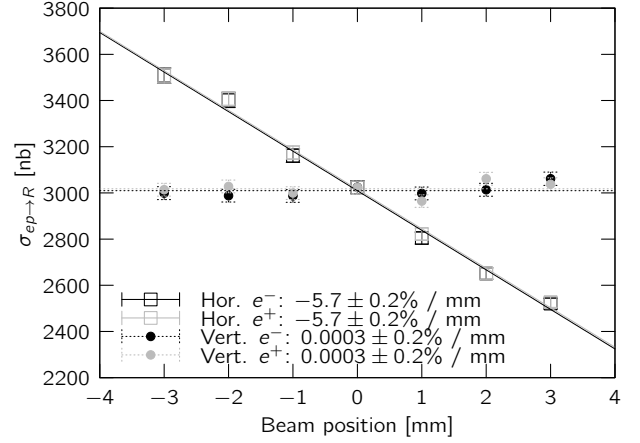


Figure 4: Simulation indicates that the cross-section $\sigma_{ep \rightarrow R}$ is unaffected by changes in the beam's vertical position, but changes in the horizontal position have a 5.7%/mm effect, which is independent of beam species.

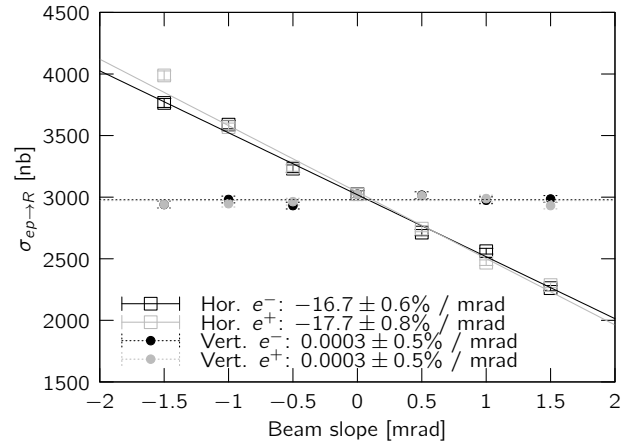


Figure 5: Simulation indicates that the cross-section $\sigma_{ep \rightarrow R}$ is unaffected by changes in the beam's vertical slope, but changes in the horizontal slope have a 17%/mrad effect, which is nearly independent of beam species.

The largest source of systematic uncertainty came from uncertainty in the beam position monitors (BPMs). OLYMPUS used two BPMs, one upstream and one downstream of the scattering chamber to locate the beam position and direction as it passed through the target. This information was used as input to the simulation, so uncertainty from the BPM measurements could propagate through the simulation to $\sigma_{ep \rightarrow R}$. As seen in Figs. 4 and 5, $\sigma_{ep \rightarrow R}$ was relatively insensitive to changes in the beam's vertical position and slope, but changes to the beam's horizontal position and slope could produce large effects on the cross-section. However, to produce an error in the relative luminosity determination, an inaccuracy in the beam position would need to be charge-asymmetric. There are two ways in which this could occur:

1. Inaccuracy of the BPM survey, coupled with different average positions for the e^+ and e^- beams,
2. Charge-dependent inaccuracy in the BPMs.

In the case of the former, the accuracy of the BPM measurements was only as good as our knowledge of the position and orientation of the BPMs themselves. The BPMs were measured during the OLYMPUS optical survey, and while this survey constrained their positions to better than 0.2 mm, the uncertainty of the orientation of the BPM axes was conservatively estimated to be 0.5 mm of displacement at a radius of 55 mm, i.e., $\approx 0.52^\circ$. During OLYMPUS running, the e^+ beam had an average vertical offset of 0.14 mm in position and 0.44 mrad in slope relative to the e^- beam. Due to uncertainty in the BPM orientation, these could couple to horizontal shifts of 1.3 μm and 1.9 μrad , and introduce uncertainties (according to the simulation results in figures 4 and 5) of 0.007% and 0.034%.

To assess the charge-dependent accuracy of the BPMs, we used the residuals of fits to charge-independent calibration data to set an upper bound for any charge-asymmetric effects. We made the conservative assumption that the non-linearity of these fits, when taken over the full range of possible beam positions, could contribute 100% to the charge-asymmetric uncertainty. Therefore, we estimate that the individual BPMs could have a charge-asymmetric inaccuracy of no greater than 10 μm , and that the readout system could produce a fully correlated charge-asymmetric inaccuracy of no greater than 20 μm . The former case could produce a position offset of 7 μm (0.04% uncertainty) and a slope offset of 10 μrad (0.17% uncertainty). The latter case could produce a 20 μm horizontal position offset introducing an uncertainty of 0.11%. Combining all of the associated uncertainties in quadrature, we find that the BPM uncertainty on the species-relative luminosity is 0.21%.

4.2. Magnetic Field at the Target

The beam position and slope at the target were inferred by assuming a straight-line trajectory of the beam between the BPMs. However, residual magnetic fields in the target region (described in section 6.2 of [5]) must have produced a slight but opposite curvature for the trajectories of the e^+ and e^- beams, which was unaccounted for. To estimate the size of this effect, we numerically integrated the equations of motion between the BPM positions interpolating between measurements of the magnetic field. We found that the target-region magnetic field would introduce a 3 μm offset and a 12 mrad deflection between the e^- and e^+ beam, corresponding to an uncertainty of 0.20%.

4.3. Collimator Geometry

The simulation made assumptions about the geometry of the SYMB detectors, most crucially the position and orientation of the collimator aperture for the right calorimeter, which defines the acceptance when simulating $\sigma_{ep \rightarrow R}$. The collimator placement in simulation was informed by the results of the OLYMPUS optical survey. Since the residual magnetic field in the region of the downstream beam pipe bends electrons and

positrons in opposite directions, geometry error can produce error in the species-relative luminosity.

We estimated this error by simulating $\sigma_{ep \rightarrow R}$ for many different positions and orientations of the right collimator. We found that the dependence on the horizontal position was 0.13%/mm and was smaller than 0.10%/mm on the vertical position. Moving the collimator forwards and backwards had a negligible effect on $\sigma_{ep \rightarrow R}$. We gauged the accuracy of the collimator position and orientation using residuals of fits to the optical survey data, conservatively estimating the position to be accurate to within 0.5 mm, producing uncertainties of 0.07% and 0.05% respectively. We found that a rotation about the horizontal axis (moving the face of the collimator up or down) produced a change of 0.27%/deg., while a rotation about the vertical axis (moving the face of the collimator left or right) produced a change of 0.40%/deg. We conservatively estimated that the collimator orientations were accurate to within 0.2° , producing uncertainties of 0.05% and 0.08% respectively. Adding these uncertainties in quadrature gives a total of 0.13% on the species relative luminosity.

4.4. Event Selection

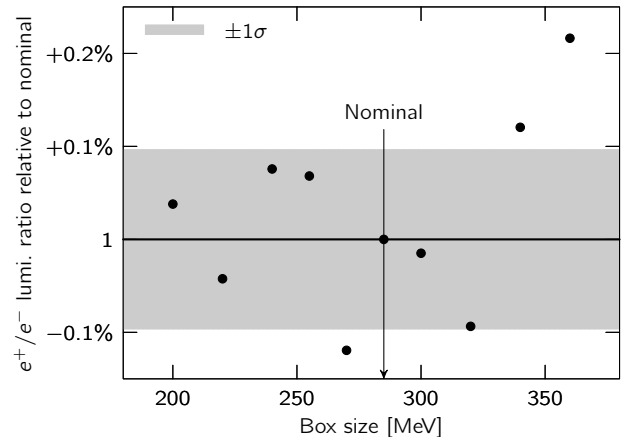


Figure 6: Adjusting the size of the box-cut region produces a change in the extracted luminosity ratio of only $\pm 0.10\%$.

The total number of counts within the various SYMB signal peaks was estimated by integrating over a box-shaped region of the spectrum shown in Fig. 2. Boxes were used for simplicity after it was shown that shape of the integration region had negligible effect on the total number of counts, so long as the size of the region was large enough. The signal peaks are well isolated and there is a negligible contribution from background. We used the same size boxes for both the (1, 1) and (1, 3) peaks.

To evaluate the effect of our event selection on the extracted luminosity ratio, the ratio was calculated for many different sizes of box cuts, both larger and smaller than the nominal size. The results are shown in Fig. 6. The standard deviation of the extracted luminosity ratios was 0.10%, which we quote for the systematic uncertainty due to event selection.

4.5. Downstream Magnetic Field

Though the OLYMPUS toroid magnet was designed to keep the magnetic field in the beamline region to a minimum, there was some residual stray field, which caused the trajectories of electrons and positrons to bend before entering the SYMBs. This bending is accounted for in the simulation, but uncertainty in the accuracy of the simulated field model propagates through the simulation to uncertainty in $\sigma_{ep \rightarrow R}$. The effect of the magnetic field was studied in simulation and found to produce a 0.53% change in the extracted luminosity ratio relative to a zero-field simulation. We conservatively estimate that our simulation models the effects of this field correctly to within 10%, and we quote a systematic uncertainty on the luminosity ratio of 0.05%.

4.6. Higher-Order Corrections

In the derivation of eq. 13, we have neglected terms of higher order than σ^2 . Based on Fig. 3, this approximation is justified, but we conservatively quote an uncertainty of 0.05% for the effect of these neglected terms.

4.7. Radiative Corrections

The simulation of $\sigma_{ep \rightarrow R}^{\text{sim.}}$ used the OLYMPUS radiative event generator, which calculates a radiative ep cross-section under several different model assumptions. The luminosity was extracted using each of the various assumptions to test if there was any dependence on model. The only model choice that was found to affect the luminosity extraction was whether the corrections model was based on a $(1 + \delta)$ correction or on an exponentiated correction ($\exp(\delta)$). The full scale for this difference was 0.05% on the ratio, i.e., $\sigma_{e^+p \rightarrow R}^{\text{sim.}}/\sigma_{e^-p \rightarrow R}^{\text{sim.}}$ is 0.05% higher when exponentiating. We quote a systematic uncertainty of half that difference rounded up, i.e., 0.03%.

4.8. Beam Energy

Uncertainty in the relative beam energy between electrons and positrons produces uncertainty in the extracted luminosity, via uncertainty in $\sigma_{ep \rightarrow R}^{\text{sim.}}$. The DORIS beam energy was monitored over time by using a reference magnet, and was calibrated through a measurement of the depolarization resonance of the Sokolov-Ternov polarization of the DORIS beam (see [6] and [7] for descriptions of the technique). We estimate that the uncertainty in the relative beam energy between electrons and positrons is 500 keV, i.e., $\approx 0.025\%$. To estimate the effect on the luminosity ratio, we evaluated the change in the Rosenbluth cross-section for scattering at 1.27° for 500 keV shifts relative to a 2.01 GeV beam:

$$\delta = 1 - \frac{\sigma(E - \delta E, \theta_{\text{SYMB}})}{\sigma(E + \delta E, \theta_{\text{SYMB}})} \approx 0.10\%, \quad (14)$$

where $E = 2.01$ GeV, $\delta E = 500$ keV, and $\theta_{\text{SYMB}} = 1.27^\circ$.

However, when the luminosity determination is used to normalize a measurement of the e^+p/e^-p cross-section ratio made with the same beam (as in OLYMPUS), any deviations in the true beam energy affect the luminosity and the cross section ratio in the same direction, i.e., there is a partial cancellation of

the effect. Rather than adding a 0.10% normalization error over the entire acceptance, the effect of beam energy uncertainty on the e^+p/e^-p cross-section ratio, i.e., the main OLYMPUS result, is better described with:

$$\delta(\theta) = 1 - \frac{\sigma(E - \delta E, \theta)}{\sigma(E + \delta E, \theta)} \times \frac{\sigma(E + \delta E, \theta_{\text{SYMB}})}{\sigma(E - \delta E, \theta_{\text{SYMB}})} \quad (15)$$

This uncertainty ranges from 0.04–0.13% over the OLYMPUS acceptance, and is quoted as the beam energy uncertainty for the OLYMPUS result [2].

Since beam energy uncertainty and luminosity uncertainty are treated as separate in the OLYMPUS result, we make a similar distinction in this work. For convenience, in Table 2, we present uncertainty totals with and without the beam energy uncertainty.

5. Advantages of the MIE Method

The chief advantage of the MIE method is that its luminosity extraction comes from a ratio of two count rates, rather than a single count rate. For a systematic effect to bias the result, it must affect both count rates differently. This guards against many forms of detector inefficiency or data acquisition failures, and reduces the degree to which the extraction is vulnerable to errors in beam position, beam energy, and alignment.

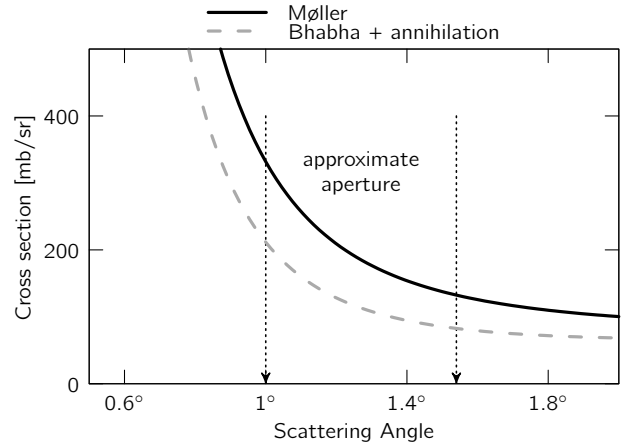


Figure 7: The cross-section for events in the SYMB calorimeters changes by almost a factor of two between electron running (black solid curve) and positron running (gray dashed curve) and has a different angular dependence. This is problematic when making a relative luminosity measurement.

A second advantage of the MIE method, which is specific to determining relative luminosity between electron and positron modes, is that the method compares numbers which are of similar size and of similar dependence on detector acceptance. This is not the case when comparing simple rates of Møller and Bhabha scattering. Fig. 7 shows the tree-level cross-sections for Møller scattering compared with Bhabha scattering (including a small contribution from pair annihilation) for a 2.01 GeV beam energy in the range of lab-frame scattering angles relevant for OLYMPUS. The Møller and Bhabha cross-sections are different by more than 60% within the SYMB acceptance.

Furthermore, Møller scattering, being t - and u -channel, has a different angular dependence from Bhabha scattering, being t - and s -channel, so that not only are the relative rates quite different, this difference depends on the exact detector acceptance. It is difficult to control systematic effects when the sensitivity to the detector acceptance is so large. By contrast, in the MIE method, the large differences between the Møller and Bhabha cross-sections cancel, while the ep process has a nearly identical cross-section for electrons and positrons. This makes the MIE method more robust.

A third advantage is that the MIE method does not rely strongly on simulations of the Møller or Bhabha acceptance. These acceptances cancel between $N_{(1,3)}$ and $N_{(1,1)}$, and so there is no opportunity for simulation errors to affect the luminosity determination via these terms.

Future electron- (and/or positron-) scattering experiments using calorimetry to monitor luminosity between running modes can take advantage of this MIE technique as a means to guard against or reduce systematic effects. The method employed in OLYMPUS made use of the (1,1) and (1,3) signal peaks that were available within the dynamic range of the SYMB ADCs. However, a luminosity monitor designed with the MIE method in mind should be built to cover many different multi-interaction peaks—(2,2), (3,1), (2,0), etc.—for cross checks and to reduce uncertainties.

6. Summary

In this paper, we have presented a method for extracting the relative luminosity between two running modes using multi-interaction events. This method was used to determine the relative luminosity between electron and positron datasets in the OLYMPUS experiment [2] and achieved better accuracy than the method of comparing Møller and Bhabha rates alone. For the specific case of OLYMPUS, we estimate that the method is accurate to within 0.36% for a determination of the relative luminosities. The chief advantage of this method, comparing ratios of rates rather than rates directly, can easily generalize to other calorimetric luminosity monitors for future electron or positron scattering experiments.

7. Acknowledgements

We gratefully acknowledge the other members of the OLYMPUS collaboration, who guided the development of this work. Discussions with Douglas Hasell, Michael Kohl, Robert Redwine, Uwe Schneekloth, Frank Maas, Dmitry Khanef, Rebecca Russell, Brian Henderson, Lauren Ice, and Jürgen Diefenbach were greatly appreciated. We wish to thank Frank Brinker and Uwe Schneekloth at DESY, who made possible the DORIS beam energy calibration.

This work was supported by the Office of Nuclear Physics of the U.S. Department of Energy, grant No. DE-FG02-94ER40818.

References

- [1] R. Milner, D. Hasell, M. Kohl, U. Schneekloth, N. Akopov, et al., The OLYMPUS Experiment, Nuclear Instruments and Methods in Physics Research Section A: Accelerators, Spectrometers, Detectors and Associated Equipment 741 (2014) 1–17.
- [2] B. Henderson, et al., Hard Two-Photon Contribution to Elastic Lepton-Proton Scattering: Determined by the OLYMPUS Experiment, Phys. Rev. Lett. accepted (2016).
- [3] R. Pérez Benito, D. Khanef, C. O'Connor, L. Capozza, J. Diefenbach, B. Gläser, Y. Ma, F. Maas, D. R. Piñeiro, Design and Performance of a Lead Fluoride Detector as a Luminosity Monitor, Nucl. Instrum. Meth. A826 (2016) 6–14.
- [4] T. Benisch, S. Bernreuther, E. Devitsin, V. Kozlov, S. Potashov, K. Rith, A. Terkulov, C. Weiskopf, The luminosity monitor of the HERMES experiment at DESY, Nucl. Instrum. Meth. A471 (2001) 314–324.
- [5] J. C. Bernauer, et al., Measurement and tricubic interpolation of the magnetic field for the OLYMPUS experiment, Nucl. Instrum. Meth. A823 (2016) 9–14.
- [6] C. Steier, J. Byrd, P. Kuske, Energy calibration of the electron beam of the ALS using resonant depolarization, in: Particle accelerator. Proceedings, 7th European Conference, EPAC 2000, Vienna, Austria, June 26-30, 2000. Vol. 1-3, pp. 1566–1568.
- [7] S. C. Leemann, M. Boege, M. Dehler, V. Schlott, A. Streun, Precise beam energy calibration at the SLS storage ring, in: Particle accelerator. Proceedings, 8th European Conference, EPAC 2002, Paris, France, June 3-7, 2002, pp. 662–664.